Inorg. Chem. **2006**, *45*, 6048–6055

Hydrogen Atom Abstraction by a Mononuclear Ferric Hydroxide Complex: Insights into the Reactivity of Lipoxygenase

Christian R. Goldsmith and T. Daniel P. Stack*

Department of Chemistry, Stanford University, California 94305

Received April 12, 2006

The lipoxygenase mimic $[Fe^{III}(\mathbf{PY5})(OH)](CF_3SO_3)_2$ is synthesized from the reaction of $[Fe^{II}(\mathbf{PY5})(MeCN)](CF_3SO_3)_2$ with iodosobenzene, with low-temperature studies suggesting the possible intermediacy of an Fe(IV) oxo species. The Fe(III)–OH complex is isolated and identified by a combination of solution and solid-state methods, including EPR and IR spectroscopy. $[Fe^{III}(\mathbf{PY5})(OH)]^{2+}$ reacts with weak X–H bonds in a manner consistent with hydrogen-atom abstraction. The composition of this complex allows meaningful comparisons to be made with previously reported Mn(III)–OH and Fe(III)–OMe lipoxygenase mimics. The bond dissociation energy (BDE) of the O–H bond formed upon reduction to $[Fe^{II}(\mathbf{PY5})(H_2O)]^{2+}$ is estimated to be 80 kcal mol^{-1}, 2 kcal mol^{-1} lower than that in the structurally analogous $[Mn^{II}(\mathbf{PY5})(H_2O)]^{2+}$ complex, supporting the generally accepted idea that Mn(III) is the thermodynamically superior oxidant at parity of coordination sphere. The identity of the metal has a large influence on the entropy of activation for the reaction with 9,10-dihydroanthracene; $[Mn^{III}(\mathbf{PY5})(OH)]^{2+}$ has a 10 eu more negative $\Delta S^{\ddagger}$ value than either $[Fe^{III}(\mathbf{PY5})(OH)]^{2+}$ or $[Fe^{III}(\mathbf{PY5})(OMe)]^{2+}$, presumably because of the increased structural reorganization that occurs upon reduction to $[Mn^{II}(\mathbf{PY5})(H_2O)]^{2+}$. The greater enthalpic driving force for the reduction of Mn(III) correlates with $[Mn^{III}(\mathbf{PY5})(OH)]^{2+}$ reacting more quickly than $[Fe^{III}(\mathbf{PY5})(OH)]^{2+}$. Curiously, $[Fe^{III}(\mathbf{PY5})(OMe)]^{2+}$ reacts with substrates only about twice as fast as $[Fe^{III}(\mathbf{PY5})(OH)]^{2+}$, despite a 4 kcal mol^{-1} greater enthalpic driving force for the methoxide complex.

Introduction

Metal-based proton-coupled electron transfer (PCET) from organic substrates is a subject of great interest, having been invoked in the oxidative mechanisms of several coordination complexes and metalloenzymes.[1,2] The generally accepted rate-determining step (RDS) in the enzymatic mechanism of lipoxygenases (LOs) entails a mononuclear non-heme Fe(III)−OH species abstracting a net hydrogen atom from an unsaturated fatty acid to produce an allylic radical and an Fe(II)−H_2O species.[3] An intriguing aspect of this mechanism is that the C−H activation of a relatively strong C−H group is achieved without invoking a high-valent iron oxidation state. A genetically homologous manganese-containing LO (Mn-LO), only discovered in 1998, is believed to react through a similar rate-determining PCET mechanism, described as a hydrogen-atom abstraction (HA) mechanism, for its reaction with linoleic acid has an analogously high kinetic isotope (H/D) effect.[4] Numerous inorganic complexes are thought to activate C−H bonds in a manner similar to the LOs, yet the factors that mediate the rate of PCET among these metal-based oxidants are not well understood.

The reactivity of $[Fe^{III}(\mathbf{PY5})(OMe)]^{2+}$ (**PY5** = 2,6-bis-(bis(2-pyridyl)methoxymethane)pyridine) with hydrocarbon substrates provides chemical precedence for an Fe(III)−OR complex activating a C−H bond, similar to the mechanism generally accepted for LOs. This ferric complex is reduced to $[Fe^{II}(\mathbf{PY5})(MeOH)]^{2+}$ by hydrocarbon substrates with weak C−H bonds (<88 kcal mol^{-1}).[5,6] The O−H bond formed upon reduction is estimated to have a bond dissociation energy (BDE) of 84 kcal mol^{-1}.[5] Although this BDE is larger than those of many other O−H bonds formed upon

* To whom correspondence should be addressed. Phone: (650) 725-8736. Fax: (650) 725-0259. E-mail: stack@stanford.edu.

(1) Cukier, R. I. *J. Phys. Chem. B* **2002**, *106*, 1746−1757.
(2) Stubbe, J.; Nocera, D. G.; Yee, C. S.; Chang, M. C. Y. *Chem. Rev.* **2003**, *103*, 2167−2201.
(3) Nelson, M. J.; Seitz, S. P. In *Active Oxygen in Biochemistry*; Valentine, J. S., Foote, C., Greenberg, A., Liebman, J. F., Ed.; Blackie Academic & Professional: London, 1995; Vol. 3, pp 276−312.
(4) Hamberg, M.; Su, C.; Oliw, E. *J. Biol. Chem.* **1998**, *273*, 13080−13088.
(5) Goldsmith, C. R.; Jonas, R. T.; Stack, T. D. P. *J. Am. Chem. Soc.* **2002**, *124*, 83−96.
(6) Jonas, R. T.; Stack, T. D. P. *J. Am. Chem. Soc.* **1997**, *119*, 8566−8567.

10.1021/ic060621e CCC: $33.50
Published on Web 06/23/2006

Scheme 1

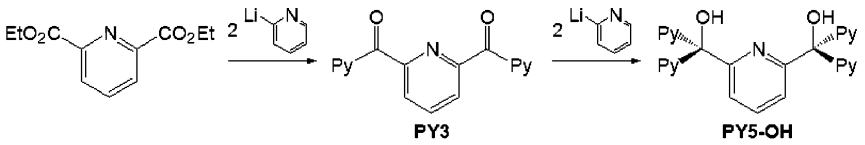

the reduction of metal-based oxidants, the Fe(III)−OMe complex reacts with hydrocarbon substrates almost 100 times more slowly than anticipated on the basis of the correlation of rate constants with BDE.[7] Analogous C−H activation is found for $[Mn^{III}(\mathbf{PY5})(OH)]^{2+}$, which was investigated to explore the feasibility of a Mn-LO with a similar coordination sphere to the Fe-LOs.[8] The O−H bond formed upon reduction to $[Mn^{II}(\mathbf{PY5})(H_2O)]^{2+}$ is estimated to have a BDE of 82 kcal mol^{-1}.[8] Although the enthalpic driving force for the oxidation of substrate is slightly lower for $[Mn^{III}(\mathbf{PY5})(OH)]^{2+}$, it reacts more rapidly than the Fe(III)−OMe complex under most conditions, suggesting that other factors in addition to the enthalpic driving force modulate the reactivity. As with the Fe(III)−OMe complex, the Mn(III)−OH complex reacts more slowly than anticipated from the BDE of the OH bond in its reduced form.[8] Unfortunately, neither the exogenous ligand nor the metal center is conserved between the complexes, precluding further analysis of the factors that modulate the reactivity.

Presented here are the synthesis and characterization of $[Fe^{III}(\mathbf{PY5})(OH)]^{2+}$, which is chemically analogous to both $[Fe^{III}(\mathbf{PY5})(OMe)]^{2+}$ and $[Mn^{III}(\mathbf{PY5})(OH)]^{2+}$. This complex reacts with hydrocarbon substrates in a manner consistent with HA, with rates of reduction that are similar to those of the previously reported **PY5** oxidants. The ability to directly compare $[Fe^{III}(\mathbf{PY5})(OH)]^{2+}$ to the other **PY5**-based oxidants facilitates the analysis of the various thermodynamic and kinetic influences on the rate of the oxidation of substrates by HA and other PCET mechanisms.

Results

Ligand Synthesis. The **PY5-OH** precursor to the 2,6-bis-(bis(2-pyridyl)methoxy-methane)pyridine ligand (**PY5**) was synthesized previously from the reaction of 4 equiv of 2-lithiopyridine with the diacid chloride of 2,6-pyridinedicarboxylic acid. This capricious reaction often leads to many byproducts that are removed by extensive chromatography. An alternate two-step synthesis to **PY5-OH** (Scheme 1) through **PY3**, a crystalline species, is presented, which simplifies the large-scale preparation of the **PY5** ligand.

Metal Complex Syntheses. The solution behavior of all iron complexes relevant to this study is summarized in Scheme 2, and the abbreviations of the metal complexes can be found in Scheme 3. The metal complexes $Fe^{II}\mathbf{L}H_2O$ and $Fe^{II}\mathbf{L}$MeCN were prepared previously.[5,6,9] A synthetic route to $Fe^{III}\mathbf{L}$OH analogous to that used to prepare $Mn^{III}\mathbf{L}$OH was followed.[8] One equivalent of iodosobenzene (C_6H_5IO) and

Scheme 2

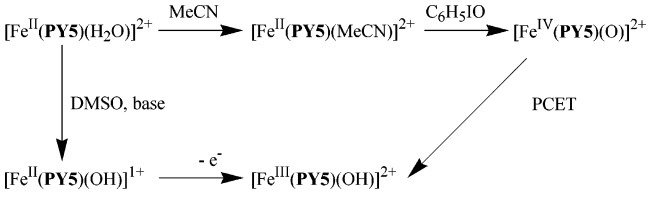

Scheme 3

$[Fe^{II}(\mathbf{PY5})(MeCN)](CF_3SO_3)_2$	$Fe^{II}\mathbf{L}$MeCN
$[Fe^{II}(\mathbf{PY5})(MeOH)](CF_3SO_3)_2$	$Fe^{II}\mathbf{L}$MeOH
$[Fe^{III}(\mathbf{PY5})(OMe)](CF_3SO_3)_2$	$Fe^{III}\mathbf{L}$OMe
$[Fe^{II}(\mathbf{PY5})(H_2O)](CF_3SO_3)_2$	$Fe^{II}\mathbf{L}H_2O$
$[Fe^{II}(\mathbf{PY5})(OH)](CF_3SO_3)_2$	$Fe^{II}\mathbf{L}$OH
$[Fe^{III}(\mathbf{PY5})(OH)](CF_3SO_3)_2$	$Fe^{III}\mathbf{L}$OH
$[Fe^{IV}(\mathbf{PY5})(O)](CF_3SO_3)_2$	$Fe^{IV}\mathbf{L}$O
$[Mn^{II}(\mathbf{PY5})(H_2O)](CF_3SO_3)_2$	$Mn^{II}\mathbf{L}H_2O$
$[Mn^{III}(\mathbf{PY5})(OH)](CF_3SO_3)_2$	$Mn^{III}\mathbf{L}$OH

$Fe^{II}\mathbf{L}$MeCN are mixed in MeCN at room temperature (RT). After 120 min, the solution is filtered and concentrated to isolate $Fe^{III}\mathbf{L}$OH as a reddish powder in a high yield (>90%). If an excess of C_6H_5IO is added to $Fe^{II}\mathbf{L}$MeCN at RT, a transient green color is observed prior to conversion to $Fe^{III}\mathbf{L}$OH. At lower temperature and with the more soluble oxygen atom-transfer agent *meta*-chloroperbenzoic acid (MCPBA), an ephemeral UV−vis feature is observed at 710 nm (∼500 M^{-1} cm^{-1}, Figure 1). The 710 nm species is

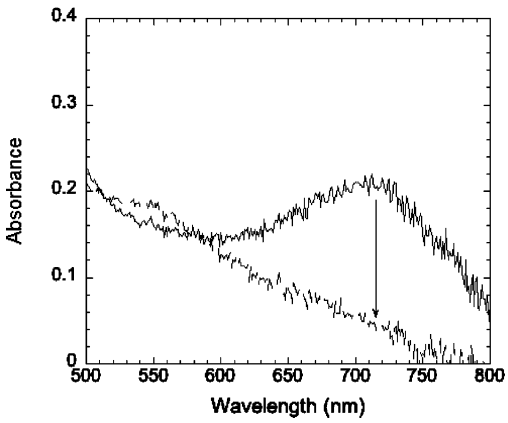

Figure 1. Spectrum of species tentatively identified as $Fe^{IV}\mathbf{L}$O (solid line). The dashed spectrum shows the reduction of $Fe^{IV}\mathbf{L}$O by 9,10-dihydroanthracene in MeCN under N_2 at 233 K.

tentatively identified as $Fe^{IV}\mathbf{L}$O because of its optical similarity to the recently characterized Fe(IV) oxo complexes.[10−12] Yet, $Fe^{IV}\mathbf{L}$O forms much more slowly than other reported Fe(IV) oxo complexes; the formation of $Fe^{IV}\mathbf{L}$O occurs over several hours at 233 K, a temperature at which most Fe(IV) oxo complexes form within 2 min.[10−12] The rate of formation

(7) Roth, J. P.; Mayer, J. M. *Inorg. Chem.* **1999**, *38*, 2760−2761.
(8) Goldsmith, C. R.; Cole, A. P.; Stack, T. D. P. *J. Am. Chem. Soc.* **2005**, *127*, 9904−9912.
(9) Goldsmith, C. R.; Jonas, R. T.; Cole, A. P.; Stack, T. D. P. *Inorg. Chem.* **2002**, *41*, 4642−4652.
(10) Kaizer, J.; Costas, M.; Que, L., Jr. *Angew. Chem., Int. Ed.* **2003**, *42*, 3671−3673.

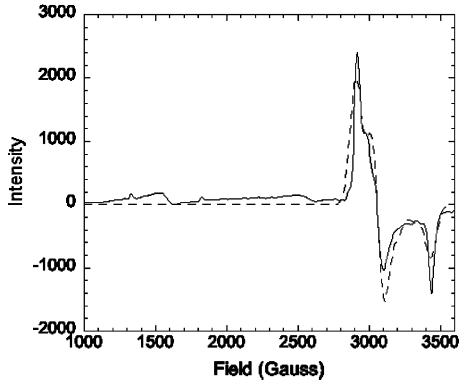

Figure 2. X-band EPR spectrum of Fe^{III}**L**OH in MeCN at 77 K (solid line) overlaid with the calculated spectrum used to fit the data (dashed line). For the low-spin component, $g = 2.30$, 2.18, and 1.94.

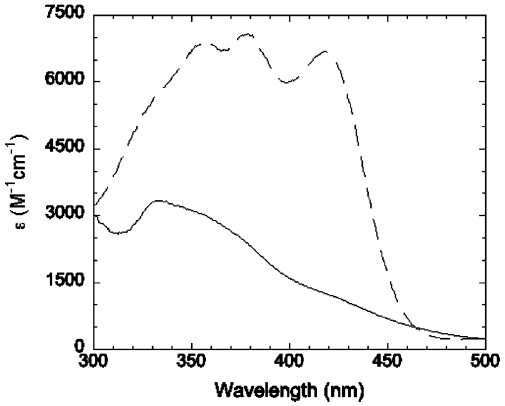

Figure 3. Comparative UV−vis spectra of Fe^{III}**L**MeCN (dashed line) and Fe^{III}**L**OH (solid line) in MeCN at RT.

can be accelerated by warming the solution, although this also hastens its decomposition. Fe^{IV}**L**O is unstable at all examined temperatures, with an exponential rate of decay of ca. 1×10^{-4} s^{-1} ($t_{1/2} \approx 90$ min) at 233 K. The final iron-based product has UV−vis features consistent with Fe^{III}**L**OH (vide infra).[5] The conversion of Fe^{IV}**L**O to Fe^{III}**L**OH occurs within 2 min of the addition of 1 equiv of 9,10-dihydroanthracene (DHA) at 233 K (Figure 1) or 1,4-cyclohexadiene. The addition of 10 equiv of 2,4,6-tri-*tert*-butylphenol (TTBP) to a 233 K solution of Fe^{IV}**L**O in MeCN results in the immediate formation of the phenoxyl radical, as identified by optical spectroscopy. The reaction between Fe^{III}**L**OH and TTBP to form Fe^{II}**L**H$_2$O is slow at this temperature, and the production of the radical coincides with the reduction of Fe^{IV}**L**O. Consequently, none of the optical features associated with Fe^{II}**L**MeCN are observed.[5] At RT, Fe^{IV}**L**O is generated transiently with an excess of MCPBA and reduces to an Fe(III) species with a k_{obs} value of 6.5×10^{-4} s^{-1}. The analogous reduction in MeCN-d_3 is slower with $k_{obs} = 3.7 \times 10^{-4}$ s^{-1}. Interestingly, the Fe^{IV}**L**O species does not epoxidize *cis*-cyclooctene readily. The addition of 100 equiv of *cis*-cyclooctene at 233 K does not hasten the disappearance of Fe^{IV}**L**O, and only trace amounts of *cis*-cyclooctene oxide are detected after the solution is warmed to RT (<0.1 equiv relative to the amount of Fe^{IV}**L**O in solution).

Solution and Solid-State Characterization. The solution magnetic susceptibility[13] of Fe^{III}**L**OH was determined to be $5.2 \pm 0.3\ \mu_B$ in MeCN at RT, a value consistent with a high-spin (hs) ferric complex. The ^{1}H NMR spectrum for Fe^{III}**L**OH in MeCN-d_3 at RT has six broad peaks in the −15 to +45 ppm range. The complex apparently undergoes a spin crossover with cooling, and the EPR spectrum for Fe^{III}**L**OH in MeCN at 77 K (Figure 2) is best modeled as a rhombic low-spin (ls) Fe(III) center with $g = 2.30$, 2.18, and 1.94. As with the previously characterized Fe^{III}**L**OMe,[5] a lower-field signal at 1500 G ($g \approx 4.3$) exists that may either correspond to a hs ferric impurity or a hs component of Fe^{III}**L**OH that has not undergone spin crossover. The EPR spectrum of Fe^{III}**L**OMe in MeCN appears to be qualitatively similar but distinct from that of Fe^{III}**L**OH ($g = 2.25$, 2.17, and 1.96).[14]

Oxidation of Fe^{II}**L**MeCN to Fe^{III}**L**OH results in the loss of the intense metal-to-ligand charge-transfer features in the UV−vis spectrum corresponding to the conversion of the ls ferrous complex to the hs ferric complex (Figure 3). As anticipated, the orange MeCN solutions of Fe^{III}**L**OH have an absorption feature at 335 nm (3400 M^{-1} cm^{-1}) that resembles that observed for Fe^{III}**L**OMe (337 nm, 3600 M^{-1} cm^{-1}).[5] The energy and intensity of this feature suggest that it results from a ligand-to-metal charge-transfer transition between the pyridine ligands of **PY5** and the Fe(III) center. The cyclic voltammetry of Fe^{III}**L**OH in DMSO exhibits a reversible oxidation potential at 0.555 V vs SHE ($\Delta E = 100$ mV) that is attributed to the conversion of Fe^{III}**L**OH to Fe^{II}**L**OH.[5] The infrared spectrum of Fe^{III}**L**OH (Nujols)[14] has a sharp feature at 3398 cm^{-1}, consistent with the O−H stretch of a hydroxide ligand.

Thermodynamic Justification. The complexes Fe^{III}**L**OH and hs Fe^{II}**L**H$_2$O differ by a net hydrogen atom. The gas-phase BDE of the O−H bonds in the ligated H$_2$O in Fe^{II}**L**H$_2$O can be estimated using a thermodynamic cycle (Scheme 4) that includes the redox potential of Fe^{III}**L**OH in DMSO, the pK_a of Fe^{II}**L**H$_2$O in DMSO, the BDE of H$_2$, and the reduction potential of a proton in DMSO. The acid−base behavior of Fe^{II}**L**H$_2$O was studied in DMSO since it rapidly converts to Fe^{II}**L**MeCN in MeCN (Scheme 2, Table 1).[9] The titration of Fe^{II}**L**H$_2$O to a solution of bromocresol green[15] forms the protonated indicator and Fe^{II}**L**OH.[14] A spectrophotometric analysis of this titration yields a pK_a of 8.1 ± 0.5 for Fe^{II}**L**H$_2$O in DMSO. The last two equations in Scheme 4 describe the free energy of the formation of the hydrogen atom and its solvation in DMSO. The values are combined with the entropic contribution at 298 K into a single constant, C,[16] that has been previously estimated as

(11) Lim, M. H.; Rohde, J.-U.; Stubna, A.; Bukowski, M. R.; Costas, M.; Ho, R. Y. N.; Münck, E.; Nam, W.; Que, L., Jr. *Proc. Natl. Acad. Sci. U.S.A.* **2003**, *100*, 3665−3670.
(12) Rohde, J.-U.; In, J.-H.; Lim, M. H.; Brennessel, W. W.; Bukowski, M. R.; Stubna, A.; Münck, E.; Nam, W.; Que, L., Jr. *Science* **2003**, *299*, 1037−1039.
(13) Evans, D. F. *J. Chem. Soc.* **1959**, 2003−2005.
(14) See Supporting Information.
(15) Kolthoff, I. M.; Chantooni, M. K., Jr.; Bhowmik, S. *J. Am. Chem. Soc.* **1968**, *90*, 23−28.
(16) Bordwell, F. G.; Cheng, J. P.; Harrelson, J. A., Jr. *J. Am. Chem. Soc.* **1988**, *110*, 1229−1231.

Scheme 4

		Energy (kcal mol^{-1})
$[Fe^{II}(\mathbf{PY5})(H_2O)]^{2+}$ (g)	$\longrightarrow$ $[Fe^{II}(\mathbf{PY5})(H_2O)]^{2+}$ (s)	ΔG^1_{solv}[a]
$[Fe^{II}(\mathbf{PY5})(H_2O)]^{2+}$ (s)	$\longrightarrow$ $[Fe^{II}(\mathbf{PY5})(OH)]^{1+}$ (s) + H^+ (s) ($pK_a = 8.1$)	11.1
$[Fe^{II}(\mathbf{PY5})(OH)]^{1+}$ (s)	$\longrightarrow$ $[Fe^{III}(\mathbf{PY5})(OH)]^{2+}$ (s) + e^- ($E_{pc} = 0.555$ V)	12.8
$[Fe^{III}(\mathbf{PY5})(OH)]^{2+}$ (s)	$\longrightarrow$ $[Fe^{III}(\mathbf{PY5})(OH)]^{2+}$ (g)	$-\Delta G^2_{solv}$[a]
H^+ (s) + e^-	$\longrightarrow$ $^1/_2\,H_2$ (g)	C = 56.0[b]
$^1/_2\,H_2$ (g)	$\longrightarrow$ H• (g)	
$[Fe^{II}(\mathbf{PY5})(H_2O)]^{2+}$ (g)	$\longrightarrow$ $[Fe^{III}(\mathbf{PY5})(OH)]^{2+}$ (g) + H• (g)	**80**

[a] ΔG^1_{solv} assumed to be equal to ΔG^2_{solv}. [b]This constant contains the entropic contribution to the free energy associated with the solvation of a hydrogen atom in DMSO. Subtraction of this term from the sum of the free energies above gives the resulting enthalpic bond dissociation energy. [c]Species followed by the notation *s* are in DMSO solution, while those followed by the notation *g* are gaseous. The value for *C* was previously reported.[17]

Table 1. Stability of **PY5**-based Oxidants (and their Reduced HA Partners) in Organic Solvents[a]

complex	MeOH	MeCN	DMSO
$[Fe^{II}(\mathbf{PY5})(MeOH)]^{2+}$	√	E	E
$[Fe^{III}(\mathbf{PY5})(OMe)]^{2+}$	√	√	E
$[Mn^{II}(\mathbf{PY5})(H_2O)]^{2+}$	D	√	D
$[Mn^{III}(\mathbf{PY5})(OH)]^{2+}$	D	√	D
$[Fe^{II}(\mathbf{PY5})(H_2O)]^{2+}$	E	E	√
$[Fe^{III}(\mathbf{PY5})(OH)]^{2+}$	E	√	√

[a] √ = stable in solution; E = monodentate ligand replaced by solvent or adventitious water; D = **PY5** dissociates from metal, as determined by ^{1}H NMR.

56 kcal mol^{-1}.[17] Summation of the equations yields an enthalpic gas-phase BDE of 80 ± 2 kcal mol^{-1} for the O−H bonds in $Fe^{II}\mathbf{L}H_2O$.

Oxidation of Substrates. In MeCN, $Fe^{III}\mathbf{L}OH$ reduces to $Fe^{II}\mathbf{L}H_2O$ in the presence of substrates with weak C−H and O−H bonds. This reduction is followed by axial ligand exchange of the nascent water ligand to yield $Fe^{II}\mathbf{L}$MeCN as a final product. The addition of 10 equiv of TTBP to a solution of $Fe^{III}\mathbf{L}OH$ at RT causes the EPR signal of $Fe^{III}\mathbf{L}OH$ to disappear, concomitant with the appearance of a $g \approx 2.0$ signal, presumably from the TTBP radical.[14] The optical bands of the TTBP radical and $Fe^{II}\mathbf{L}$MeCN overlap, precluding simple detection of the organic radical by UV−vis spectroscopy. $Fe^{III}\mathbf{L}OH$ is also reduced in the presence of substrates possessing weak C−H bonds. Reactions with DHA, xanthene, fluorene, and ethylbenzene were analyzed at 323 K. The reaction of $Fe^{III}\mathbf{L}OH$ with an excess of DHA produces nearly 0.5 equiv of anthracene for each equivalent of reduced $Fe^{III}\mathbf{L}OH$. The analogous reaction with xanthene produces traces of bixanthene (∼5%). In the presence of O_2, the reaction of $Fe^{III}\mathbf{L}OH$ with xanthene produces multiple equivalents of xanthone and 0.5 equiv of bixanthene, presumably the result of a radical chain mechanism propagated by organic peroxyl radicals.

With excess substrate, the anaerobic decay of $Fe^{III}\mathbf{L}OH$ is first-order with respect to substrate concentration for all four substrates examined. The measured k_{obs} does not change as the concentration of $Fe^{III}\mathbf{L}OH$ is varied from 0.19 to 0.40 mM with a fixed concentration of DHA (0.030 M); consequently, the RDS of the reaction is most easily interpreted as a bimolecular collision. The second-order rate constants

(17) Bordwell, F. G.; Cheng, J.-P.; Ji, G.-Z.; Satish, A. V.; Zhang, X. *J. Am. Chem. Soc.* **1991**, *113*, 9790−9795.

Table 2. Corrected Second-Order Rate Constants for the Reactions of Hydrocarbon Substrates with $[Fe^{III}(\mathbf{PY5})(OH)](CF_3SO_3)_2$ in MeCN at 298 and 323 K

substrate	k_{2corr} (298 K)[a]	k_{2corr} (323 K)[a]	KIE[b]	BDE[c]	ref[d]
xanthene		$9.1 \pm 1.0 \times 10^{-3}$		75 ± 1	17
9,10-dihydro anthracene	$4.3 \pm 0.3 \times 10^{-4}$	$2.9 \pm 0.4 \times 10^{-3}$	6.3	78 ± 2	17
fluorene		$2.7 \pm 0.2 \times 10^{-3}$		80 ± 2	17
ethylbenzene		$1.1 \pm 0.1 \times 10^{-4}$		85 ± 2	18

[a] Second-order rate constants per available C−H bond were measured at 298 and 323 K in units of M^{-1} s^{-1} and were adjusted for reaction stoichiometry to yield k_{2corr}. [b] Kinetic isotope effect determined at 298 K. [c] BDE of the weakest C−H bond in units of kcal mol^{-1}. [d] References for the BDE of the substrate.

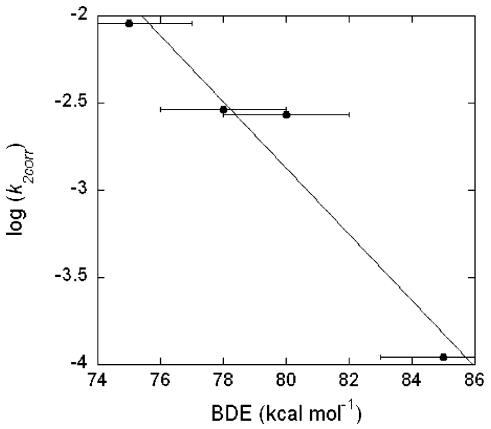

Figure 4. Dependence of k_{2corr} of the reduction of $Fe^{III}\mathbf{L}OH$ on BDE at 323 K in MeCN. All data taken with greater than 40-fold excess of substrate under anaerobic conditions. A standard ±2 kcal mol^{-1} uncertainty is displayed for all substrate BDEs.

for all hydrocarbon substrates at 323 K are statistically corrected for the number of equivalently weak C−H bonds. The rate constants are further corrected for the anticipated reaction stoichiometry in instances when the intermediate hydrocarbon radical can react with an additional equivalent of $Fe^{III}\mathbf{L}OH$ to form an aromatic or olefin product (DHA to anthracene, ethylbenzene to styrene). The fully corrected second-order rate constants are denoted k_{2corr} (Table 2). At 323 K, a linear relationship is found between log(k_{2corr}) and substrate BDE (Figure 4), while the correlation between log(k_{2corr}) and substrate pK_a is poor.[14]

The reaction of $Fe^{III}\mathbf{L}OH$ with DHA was studied in greater detail. A kinetic isotope effect (KIE) was measured with parallel reactions of DHA and DHA-d_4 at 298 K. The KIE of 6.3 implicates C−H bond cleavage in the RDS of the

Table 3. Reaction Parameters for Reactivity with 9,10-Dihydroanthracene[a]

complex	$\Delta H^{\circ b,c}$	$\Delta H^{\ddagger c}$	$\Delta S^{\ddagger d}$	ref
$[Fe(Hbim)(H_2bim)_2]^{2+}$	+2	11.6	−36	7
$[MnO_4]^{1-}$	−2	13.8	−15	22
$[L_2Mn(O)_2MnL_2]^{3+}$	−1	14.5	−23	23
$[L_2Mn(O)(OH)MnL_2]^{3+}$	+3	16	−21	23
Fe^{III}**L**OH	−2	13.2	−26	this work
Fe^{III}**L**OMe	−6	13.4	−25	5
Mn^{III}**L**OH	−4	9.3	−36	8

[a] Measured in MeCN under anaerobic conditions over the temperature range of 298−343 K. [b] Energy of the X−H bond formed upon reduction of the metal complex relative to the BDE of dihydroanthracene (78 kcal mol^{-1}). [c] Measured in kcal mol^{-1}. [d] Measured in eu.

reaction. The rate of reduction of Fe^{III}**L**OH by DHA was measured over the temperature range of 298−343 K. The variable temperature data are consistent with $\Delta H^{\ddagger} = 13.2 \pm 0.5$ kcal mol^{-1} and $\Delta S^{\ddagger} = -26 \pm 5$ eu for the reaction.[14]

Discussion

Many metalloenzymes are hypothesized to oxidize organic substrates by a proton-coupled electron-transfer (PCET) mechanism. Most of these enzymes are proposed to do this with a high-valent metal species; the binuclear iron active site of soluble methane monooxygenase, for instance, is believed to use an active Fe(IV) species to remove a hydrogen atom from methane.[19] Fe-lipoxygenases (LOs), conversely, are proposed to perform a hydrogen atom abstraction (HA) in the rate-limiting step of the mechanism from fatty acid substrates using a ferric mononuclear non-heme species.[3]

Over the past several years, numerous coordination compounds have been reported to perform PCET (Table 3). Included among these complexes are Fe^{III}**L**OMe[5,6] and Mn^{III}**L**OH[8]. These were designed as mimics of the iron-containing LOs isolated from plants and animals (Fe-LOs) and the manganese-containing analogue (Mn-LO) recently isolated from a fungus.[4,20] Fe^{III}**L**OMe and Mn^{III}**L**OH react with hydrocarbon substrates containing allylic and benzylic C−H bonds in a manner consistent with HA, providing chemical precedence for the rate-determining step (RDS) proposed for Fe-LOs and Mn-LO. A comparison between the two systems is hindered by the variation of both the metal center and the exogenous ligand.

To better understand the thermodynamic and kinetic influences of the active-site metal (Mn, Fe) and active ligand (HO^-, MeO^-), the complex Fe^{III}**L**OH was synthesized and characterized. The identity of the compound is confirmed through several spectroscopic methods, including electron paramagnetic resonance (EPR), optical spectroscopy (UV−vis), magnetic susceptibility, and infrared spectroscopy (IR). The EPR, UV−vis, and solution magnetic susceptibility measurements resemble those of Fe^{III}**L**OMe,[5] while the IR spectrum has a sharp feature with an energy (3398 cm^{-1}) consistent with a hydroxide O−H stretch. Compound Fe^{III}**L**OH represents a biomimetic improvement over Fe^{III}**L**OMe, in that its coordination sphere contains an exogenous hydroxide, as proposed for the active species of Fe-LO.[21]

The oxidation of Fe^{II}**L**MeCN to Fe^{III}**L**OH proceeds through the intermediacy of a green species tentatively assigned as Fe^{IV}**L**O, on the basis of its optical spectrum. The study of Fe^{IV}**L**O is complicated by the poor solubility of iodosobenzene and its slow rate of formation at low temperatures relative to its decay rate. The use of MCPBA as the oxidant complicates matters by producing *m*-chlorobenzoic acid, but its reaction with Fe^{II}**L**MeCN results in a similar species. The intermediate Fe^{IV}**L**O is capable of activating weak O−H and C−H bonds at 233 K. In the absence of a more easily oxidized substrate, Fe^{IV}**L**O apparently abstracts a net hydrogen atom from MeCN to form Fe^{III}**L**OH, as evidenced by the k_h/k_d kinetic isotope effect (KIE) of 1.8 observed for the RT decomposition of Fe^{IV}**L**O in MeCN-h_3 and MeCN-d_3. An alternative mechanism for the formation of Fe^{III}**L**OH involves the reaction of Fe^{IV}**L**O with 1 equiv of Fe^{II}**L**MeCN to form a μ-oxo dimer intermediate $[(\mathbf{L})Fe^{III}(O)Fe^{III}(\mathbf{L})]^{4+}$ followed by hydrolysis. Such a μ-oxo species is formed with the similar ligand N4Py,[24] but semiempirical calculations suggest that such a bridged intermediate is unlikely for the **PY5** system. Experimentally measured BDEs of O−H bonds in mononuclear Fe(III)−OH and Mn(III)−OH compounds are typically higher than 100 kcal mol^{-1},[25−27] suggesting that the oxidized Fe(IV) oxo and Mn(IV) oxo species have a high enthalpic driving force for PCET. The rapid reduction of Fe^{IV}**L**O in the presence of weak C−H bonds at 233 K is consistent with this prediction. The proposed reaction mechanism of α-ketoglutarate dependent non-heme enzymes is believed to include PCET by an Fe(IV) oxo species,[28] and this report may represent small molecule precedence for such chemistry.

The BDE of the O−H bond formed upon the reduction of Fe^{III}**L**OH to Fe^{II}**L**H_2O was estimated using a thermodynamic cycle of measurements in DMSO. The BDEs of the O−H bonds in Fe^{II}**L**MeOH and Mn^{II}**L**H_2O were calibrated in MeOH and MeCN, respectively.[5,8] Ideally, the BDEs of the O−H bonds in these metal complexes would be measured in the same solvent, but the instabilities of the **PY5**-based oxidants and their redox partners in various solvents preclude this possibility (Table 1). For the thermodynamic analysis to be valid, both the oxidized and reduced forms of the metal

(18) McMillen, D. F.; Golden, D. M. *Annu. Rev. Phys. Chem.* **1982**, *33*, 493−532.
(19) Brazeau, B. J.; Austin, R. N.; Tarr, C.; Groves, J. T.; Lipscomb, J. D. *J. Am. Chem. Soc.* **2001**, *123*, 11831−11837.
(20) Su, C.; Oliw, E. *J. Biol. Chem.* **1998**, *273*, 13072−13079.
(21) Scarrow, R. C.; Trimitsis, M. G.; Buck, C. P.; Grove, G. N.; Cowling, R. A.; Nelson, M. J. *Biochemistry* **1994**, *33*, 15023−15035.
(22) Mayer, J. M. *Acc. Chem. Res.* **1998**, *31*, 441−450.
(23) Wang, K.; Mayer, J. M. *J. Am. Chem. Soc.* **1997**, *119*, 1470−1471.
(24) Roelfes, G.; Lubben, M.; Chen, K.; Ho, R. Y. N.; Meetsma, A.; Genseberger, S.; Hermant, R. M.; Hage, R.; Mandal, S. K.; Young, V. G., Jr.; Zang, Y.; Kooijman, H.; Spek, A. L.; Que, L., Jr.; Feringa, B. L. *Inorg. Chem.* **1999**, *38*, 1929−1936.
(25) Gupta, R.; Borovik, A. S. *J. Am. Chem. Soc.* **2003** *125*, 13234−13242.
(26) Borovik, A. S. *Acc. Chem. Res.* **2005**, *38*, 54−61.
(27) The bond dissociation energy (BDE) of the O−H bond formed upon the reduction of $[Fe(N_4Py)(O)]^{2+}$ to $[Fe(N_4Py)(OH)]^{2+}$ was calculated to be 84.0 kcal mol^{-1}. Kumar, D.; Hirao, H.; Que, L, Jr.; Shaik, S. *J. Am. Chem. Soc.* **2005**, *127*, 8026−8027.
(28) Price, J. C.; Barr, E. W.; Glass, T. E.; Krebs, C.; Bollinger, J. M., Jr. *J. Am. Chem. Soc.* **2003**, *125*, 13008−13009.

complexes must be stable. In MeOH or DMSO, **PY5** dissociates from the manganese complexes, limiting the chemistry to MeCN. The exogenous ligands of the iron compounds exchange upon changing solvent,[9] limiting their study to either DMSO (Fe^{III}**L**OH/ Fe^{II}**L**H_2O) or MeOH (Fe^{III}**L**OMe/ Fe^{II}**L**MeOH). The reactivity of Fe^{III}**L**OMe with hydrocarbon substrates proceeds at similar rates in MeCN and MeOH, suggesting that the protic solvent does not significantly impact the BDE of the O−H bond in Fe^{II}**L**MeOH. The pK_a of Fe^{II}**L**H_2O (8.1, DMSO) and the reduction potential of Fe^{III}**L**OH (0.555 V vs SHE) yield a BDE of 80 ± 2 kcal mol^{-1} for the O−H bonds in the exogenous water in Fe^{II}**L**H_2O (Scheme 4). As anticipated, manganese is the superior oxidant at parity of coordination sphere because the exchange of manganese for iron results in a 2 kcal mol^{-1} stronger bond in the reduced species.[8] The exchange of the exogenous hydroxide for a methoxide increases the enthalpic driving force by 4 kcal mol^{-1}.[5]

The Fe^{III}**L**OH complex oxidizes hydrocarbon substrates through a mechanism that is consistent with HA as the RDS. The primary k_h/k_d kinetic isotope effect (6.3) for the RT reaction with DHA implicates C−H bond cleavage in the RDS. The ability of Fe^{III}**L**OH to react with 2,4,6-tri-*tert*-butylphenol (TTBP) to generate a TTBP radical demonstrates the ability of Fe^{III}**L**OH to perform a net hydrogen-atom abstraction. The corrected second-order rate constants scale better with substrate C−H BDE (Figure 4) than C−H pK_a,[14] suggesting that the oxidation does not occur through an initial proton transfer followed by a fast electron transfer. As for Fe^{III}**L**OMe and Mn^{III}**L**OH,[5,8] the high oxidation potentials of the hydrocarbon substrates relative to the reduction potential of Fe^{III}**L**OH preclude an initial electron transfer followed by a slow proton transfer as a mechanistic possibility.[29] As with Fe^{III}**L**OMe and Mn^{III}**L**OH, the Fe(III)−OH complex reacts with DHA more slowly than anticipated on the basis of the BDE of the O−H bond formed upon its reduction,[7] supporting earlier arguments that factors other than the thermodynamic driving force modulate the rate of reaction.[5, 8]

Further analysis of the reduction of Fe^{III}**L**OH by DHA yields kinetic parameters that differ from those of Mn^{III}**L**OH. The 2 kcal mol^{-1} greater $\Delta H°$ for Mn^{III}**L**OH relative to that of Fe^{II}**L**OH partly contributes to the 4 kcal mol^{-1} lower $\Delta H^{‡}$ for Mn^{III}**L**OH. The $\Delta S^{‡}$ for Fe^{III}**L**OH is 10 eu more positive than that for Mn^{III}**L**OH. The presumably greater structural reorganizational energy of Mn^{III}**L**OH upon reduction to Mn^{II}**L**H_2O is potentially responsible for the $\Delta S^{‡}$ disparity. As the hydrogen atom is transferred to the exogenous hydroxide, three Mn−N bonds in Mn^{III}**L**OH need to simultaneously elongate to remove the Jahn−Teller distortion upon reduction.[8] These simultaneous bond elongations should lead to a transition state that is much more ordered than those of the Fe(III) oxidants because none of the Fe−N distances in Fe^{III}**L**OMe change significantly upon reduction.[5] At RT, the 10 eu more negative $\Delta S^{‡}$ raises the free-energy barrier for HA by Mn^{III}**L**OH by approximately 3 kcal mol^{-1}, relative to the other HA systems that have $\Delta S^{‡} \approx -25$ eu. This is a significant perturbation that should affect the rate of oxidation by at least an order of magnitude. The greater enthalpic driving force for Mn^{III}**L**OH relative to that of Fe^{III}**L**OH partly allows the Mn(III) compound to overcome this penalty and react with substrates more quickly than Fe^{III}**L**OH. The active site of Mn-LO should undergo similar structural changes during its redox chemistry, assuming an octahedral coordination is maintained. The small molecule comparisons suggest that Mn-LO is viable, despite the presumably greater structural rearrangement, because Mn(III) is a thermodynamically superior oxidant than Fe(III) at parity of the coordination sphere.

Although the methoxide for hydroxide substitution increases the thermodynamic driving force for metal reduction, Fe(III)-OH and Fe(III)-OMe react at approximately the same rate with DHA. The reactions between Fe^{III}**L**OMe and the hydrocarbon substrates proceed twice as fast as those with Fe^{III}**L**OH as the oxidant, suggesting that the reactivity of Fe^{III}**L**OMe does not proceed through a trace Fe(III)−OH species. The axial ligand appears to have a secondary influence on the reactivity beyond the favorability of the reaction. For the reaction to proceed, the abstracted hydrogen atom presumably develops an intimate association with the axial oxygen atom of the Fe(III) compound in the transition state. The added steric demands of the methyl group on the axial methoxide ligand in Fe^{III}**L**OMe may hinder the formation of such an association, which could account for the slower reactivity.

Summary

The oxidation of Fe^{II}**L**MeCN to Fe^{III}**L**OH proceeds through a green intermediate tentatively assigned as Fe^{IV}**L**O. The chemical composition of Fe^{IV}**L**O and Fe^{III}**L**OH differ by a net hydrogen atom, raising the possibility of proton-coupled electron transfer by an Fe(IV) oxo complex. Fe^{II}-$_I$**L**OH is a functional mimic of Fe-LOs, performing hydrogen atom abstraction (HA) with hydrocarbon substrates. Its reactivity and structure are directly comparable to those of Fe^{III}**L**OMe and Mn^{III}**L**OH. The $\Delta S^{‡}$ for HA varies among the **PY5**-based oxidants and appears to correlate to the degree of structural reorganization that occurs upon reduction. The manganese for iron substitution slightly favors HA, despite the greater number of inner-sphere changes that occur upon redox changes. The methoxide for hydroxide substitution creates a thermodynamically more favorable oxidant, yet one that reacts more slowly, presumably, because of the added steric demands of the methyl substituent, which reduces the probability of a favorable association of the substrate hydrogen atom and the oxygen atom of the complex oxidant.

Experimental Section

Syntheses. All starting materials were purchased from Aldrich and used without further purification unless noted otherwise. $Fe^{II}(CF_3SO_3)_2$ was synthesized according to a literature method.[30] All solvents and gases were of analytical grade and were purified

(29) Schlesener, C. J.; Amatore, C.; Kochi, J. K. *J. Am. Chem. Soc.* **1984**, *106*, 3567−3577.

(30) Haynes, J. S.; Sams, J. R.; Thompson, R. C. *Can. J. Chem.* **1981**, *59*, 669−678.

by literature methods. MeCN and MeCN-d_3 were distilled from CaH_2 under N_2 and stored over 4 Å molecular sieves. Anhydrous diethyl ether (ether) was stored over 4 Å molecular sieves. 9,10-Dihydroanthracene (DHA), fluorene, and xanthene were recrystallized twice from EtOH, as was DHA-d_4.[5] Ethylbenzene was dried over $CaCl_2$ and distilled prior to use. Flash column chromatography was performed using Silica Gel 60, 230−400 mesh, from EM Science (Gibbstown, NJ) using standard techniques.

Instrumentation. The ^{1}H NMR spectra were recorded on a Varian Gemini-400 (400 MHz) NMR spectrometer at room temperature (RT), and the chemical shifts are reported in parts per million downfield from an internal TMS reference. The electronic spectra at RT were measured on either a Polytec X-dap fiber optics UV−Vis diode array spectrophotometer or a Cary 50 Bio UV−vis spectrophotometer. Electronic paramagnetic resonance (EPR) spectra were recorded on a Bruker ER 220D-SRC instrument as frozen solutions at 77 K at X-band frequency in quartz tubes. EPR spectra were fit using a Bruker Simfonia 1.25. Electrochemical measurements were recorded at 500 mV/s under N_2 at RT with a Bioanalytical Systems Inc. CV-50W voltammetric analyzer, a platinum working electrode, a platinum wire auxiliary electrode, 0.1 M (n-Bu_4N)(ClO_4) supporting electrolyte, and a silver/silver chloride wire reference electrode; all potentials are referenced to the ferrocenium/ferrocene couple (in DMSO = +0.750 V vs SHE, ΔE = 100 V).[31] Solution magnetic moments were determined in MeCN-d_3 at RT by the Evans method.[13] Gas chromatography−mass spectroscopy (GC−MS) data were collected on a Hewlett-Packard 5890 system. Elemental analyses were performed by Galbraith Laboratories Inc. (Knoxville, TN). Samples were dried under vacuum for 4 h at 373 K prior to analysis.

Alternate Ligand Synthesis. The **PY5** ligand can be synthesized via an alternative route to that described in the literature (Scheme 1).[5] In this alternative synthesis, 4 equiv of lithiopyridine was added in two sequential steps, resulting in intermediate products that are easier to purify.

2,6-Bis(2-pyridyl ketone)pyridine (PY3). A THF solution (400 mL) of 2-bromopyridine (15.81 g) was cooled to 195 K, and n-BuLi (40 mL, 2.5 M in hexane) was added dropwise to keep the temperature below 218 K. The slow addition of a THF solution (100 mL) of the diethyl ester of 2,6-pyridinedicarboxylic acid (10.08 g) at 195 K was followed by quenching with MeOH (100 mL) and warming of the solution to RT. After the addition of 10% HCl (200 mL), the organic solvents were removed. The acidic solution was first washed with CH_2Cl_2, and then NaOH was added until the solution became basic. This basic aqueous solution was extracted with CH_2Cl_2, and the crude product was collected by evaporation of the CH_2Cl_2 solution. Crystallization from acetone/ether yielded an off-white crystalline solid (11.10 g, 85% yield). ^{1}H NMR (400 MHz, $CDCl_3$): δ 7.46 (2 H, t of d, J_1 = 4.1 Hz, J_2 = 1.7 Hz, 5-H of py arms (py-a)), 7.79 (2 H, t of d, J_1 = 7.7 Hz, J_2 = 1.7 Hz, 4-Hpy-a), 8.12 (1 H, t, J = 7.8 Hz, 4-H of bridging py (py-b)), 8.19 (2 H, d, J = 7.8 Hz, 3-Hpy-b), 8.31 (2 H, d, J = 7.7 Hz, 3-Hpy-a), 8.75 (2 H, d, J = 4.0 Hz, 6-Hpy-a). ^{13}C NMR (400 MHz, $CDCl_3$): δ 126.1, 127.4, 136.4, 149.2, 153.4, 153.6, 191.7. MS (FAB^+, MH^+): m/e 286.1 (EM = 285.2).

2,6-Bis(bis(2-pyridyl)carbinol)pyridine (PY5-OH). A THF solution (200 mL) of 2-bromopyridine (8.3 g) was cooled to 195 K, and n-BuLi (21 mL, 2.5 M in hexane) was added dropwise to keep the temperature below 218 K. The slow addition of a THF solution (50 mL) of **PY3** (7.15 g) at 195 K was followed by quenching with MeOH (50 mL) and warming of the solution to RT. After the addition of 10% HCl (100 mL), the organic solvents were removed. The acidic solution was first washed with CH_2Cl_2, and then NaOH was added until the solution became basic. This basic aqueous solution was extracted with CH_2Cl_2, and the crude product was collected by evaporation of the solvent. Crystallization from acetone/ether yielded an off-white crystalline solid (8.21 g, 75% yield). The ^{1}H NMR and ^{13}C NMR spectra match those previously reported for this compound.[5]

[Fe(PY5)(OH)](CF_3SO_3)$_2$ (Fe^{III}LOH). The addition of 1.0 equiv of iodosobenzene (0.054 g) to a MeCN solution (2 mL) of [Fe^{II}(**PY5**)(MeCN)](CF_3SO_3)$_2$ (0.197 g) in MeCN gave a reddish Fe(III) species at RT. After 120 min, the solution was filtered then concentrated to dryness. The reddish brown powder was washed with ether (0.175 g, 92%). Absorption spectrum (MeCN): λ_{max} (nm), ϵ (M^{-1} cm^{-1}); 335, 3400. IR (Nujols): ν(O−H) 3398 cm^{-1}. Electron paramagnetic resonance (MeCN, 77 K): g = 2.30, 2.18, 1.94. Cyclic voltammetry (DMSO): +0.555 V vs SHE (ΔE = 0.100 V). Solution magnetic moment (MeCN-d_3, 291 K): μ_{eff} = 5.2 μ_B. ^{1}H NMR (400 MHz, MeCN-d_3): δ −11.6, 17.0, 26.0, 33.2, 37.8, 40.9. Anal. Calcd for $C_{31}H_{26}N_5O_9F_6S_2Fe\cdot H_2O$: C, 43.07; H, 3.26; N, 8.10. Found: C, 43.80; H, 3.84; N, 7.39.

pK_a Measurements. The pK_a of [Fe^{II}(**PY5**)(H_2O)]$^{2+}$ was determined by spectrophotometric titrations in which a DMSO solution of [Fe^{II}(**PY5**)(H_2O)]$^{2+}$ was added to a DMSO solution of bromocresol green (pK_a = 7.3, DMSO).[15] For the titration, 14 independent spectra covering the 300−700 nm wavelength range were collected. Titration with 1 equiv of triethylamine (pK_a = 9.0) deprotonated >90% of the Fe(II)−H_2O species, while the addition of >100 equiv of 2,6-lutidine (pK_a = 4.5) did not significantly deprotonate Fe(II)−H_2O. These titrations qualitatively support the measured value of 8.0. A factor analysis in SPECFIT showed that only two colored species were present above the limit of detection since the indicator species are more intensely colored than the Fe(II) complexes. This allows the titration data to be sufficiently modeled with a single equilibrium expression. The component spectra of the two pure colored species and the equilibrium constant were refined to minimize the residual between the observed absorbance at each wavelength and that calculated from the model for all independent spectra.

Kinetic Measurements. The kinetic data were measured with a Polytec X-dap fiber optics UV−Vis diode array spectrophotometer. The reaction cell was maintained at a constant temperature using a FTS Systems Model MC480A1 multitemperature bath. MeCN solutions of Fe^{III}**L**OH were prepared in the drybox or on a N_2 line using standard Schlenk techniques directly before use. The substrate was added directly to the solvent, and the solution was transferred to the reaction vessel. A fiber optic dip-probe was inserted into the solution (path length = 0.1 or 1.0 cm), and the vessel was carefully sealed.

All kinetic runs were performed with an excess of substrate to achieve pseudo-first-order conditions for the reduction of the ferric complex. For all reactions, the reduction of Fe^{III}**L**OH to Fe^{II}**L**MeCN was monitored. The reduction of [Fe^{III}(**PY5**)(OH)]$^{2+}$ was measured over the wavelength range from 300 to 800 nm, which includes the band maxima for Fe^{III}**L**OH and Fe^{II}**L**MeCN. The substrate concentration ranged from 0.20 to 2.00 M and was adjusted to achieve a reasonable rate of Fe(III) complex reduction. The reactions were run to near completion (greater than five half-lives of Fe^{III}**L**OH) in all kinetic measurements. All reactions remained homogeneous throughout the data collection.

Spectral deconvolution and kinetic analyses (SPECFIT) determined the rate constants from the absorption data collected in the

(31) Bordwell, F. G.; Bausch, M. J. *J. Am. Chem. Soc.* **1986**, *108*, 2473−2474.

wavelength range of 300−500 nm. The rate constants were determined from absorption data collected in the wavelength range of 400−600 nm for fluorene and ethylbenzene. For each substrate, at least four measurements were made of k_{obs} with substrate concentrations ranging from 0.20 to 2.0 M. The absolute second-order rate constants, k_2, were calculated by a least-squares fitting plot of k_{obs} versus substrate concentration.

Kinetic experiments were analyzed for products following each run. The reaction mixture was concentrated to dryness, dissolved in ether, and filtered to remove the manganese and ligand. Following this workup, the following products were identified by GC/MS (starting substrate in parentheses): anthracene (DHA) and trace quantities of bixanthene (xanthene). The other organic products were likely generated in quantities below the level of detection or consumed in a solvent-related side reaction.

Acknowledgment. We are grateful to the National Institutes of Health (GM50730) and the Stanford Graduate Fellowship Fund (C.R.G.) for financial support for this work. We are grateful to Dr. Russell C. Pratt and Dr. Robert Jonas for experimental assistance and to Prof. Edward I. Solomon for use of the EPR instrument.

Supporting Information Available: Figures showing MCPBA oxidation, X-band EPR spectra, titration of a bromocresol green solution, cyclic voltammetry, infrared spectra, log(k_{2corr}) vs pK_a, and an Eyring plot. This material is available free of charge via the Internet at http://pubs.acs.org.

IC060621E